Research article

Elmina Kabouraki, Vasileia Melissinaki, Amit Yadav, Andrius Melninkaitis, Konstantina Tourlouki, Theodoros Tachtsidis, Nikolaos Kehagias, Georgios D. Barmparis, Dimitris G. Papazoglou, Edik Rafailov and Maria Farsari*

High laser induced damage threshold photoresists for nano-imprint and 3D multi-photon lithography

Abstract: Optics manufacturing technology is predicted to play a major role in the future production of integrated photonic circuits. One of the major drawbacks in the realization of photonic circuits is the damage of optical materials by intense laser pulses. Here, we report on the preparation of a series of organic–inorganic hybrid photoresists that exhibit enhanced laser-induced damage threshold. These photoresists showed to be candidates for the fabrication of micro-optical elements (MOEs) using three-dimensional multiphoton lithography. Moreover, they demonstrate pattern ability by nanoimprint lithography, making them suitable for future mass production of MOEs.

Elmina Kabouraki and **Vasileia Melissinaki** contributed equally.

*Corresponding author: **Maria Farsari**, FORTH/IESL, N. Plastira 100, Heraklion 70013, Greece, E-mail: mfarsari@iesl.forth.gr. https://orcid.org/0000-0003-2435-4156
Elmina Kabouraki and Vasileia Melissinaki, FORTH/IESL, N. Plastira 100, Heraklion 70013, Greece
Amit Yadav and Edik Rafailov, Optoelectronics and Biomedical Photonics Group, AIPT, Aston University, Birmingham B4 7ET, UK
Andrius Melninkaitis, Laser Research Center, Vilnius University, Saulėtelio al. 10, Vilnius 10223, Lithuania; and Lidaris Ltd., Saulėtekio al. 10, Vilnius LT-10223, Lithuania
Konstantina Tourlouki and Theodoros Tachtsidis, Nanotypos, VEPE Technopoli Thessaloniki, Building C2, Pylea, Thessaloniki 55535, Greece
Nikolaos Kehagias, Nanotypos, VEPE Technopoli Thessaloniki, Building C2, Pylea, Thessaloniki 55535, Greece; and NCSR Demokritos, Institute of Nanoscience and Nanotechnology, P. Grigoriou 27 & Neapoleos Str., Ag. Paraskevi 15341, Greece. https://orcid.org/0000-0002-2698-383X
Georgios D. Barmparis, Physics Department, University of Crete, Heraklion 70013, Greece
Dimitris G. Papazoglou, FORTH/IESL, N. Plastira 100, Heraklion 70013, Greece; and Materials Science and Technology Department, University of Crete, Heraklion 70013, Greece

1 Introduction

Micro-optical elements (MOEs) are ideal candidates for optical applications such as beam focusing, shaping, and steering elements [1]. Their widespread use has been hindered by their fabrication complexity and high unit cost, which traditionally includes micro-milling, micro-polishing, molding, and ion-beam finishing. Recent progress in additive manufacturing (AM) has enabled the three-dimensional (3D) printing of complex microscale structures for a variety of applications, including optical and micro-optical components. One of the highest resolution AM techniques is multiphoton lithography (MPL), which has allowed the freeform 3D printing of complex micro-optical elements and components such as complex lenses and microscopes objectives [2–4], metalenses [5, 6], stacked metasurfaces with multilevel advantages enabled by MPL [7], axicons [8], and Fabry–Perot resonator [9] on flat substrates, as well as on optical fibers [10–15].

MPL is based on the multiphoton polymerization of a transparent photopolymer [16, 17]. There is a wide variety of photosensitive materials used that can be employed, including biomolecules, organic photopolymers, and hydrogels, or organically modified ceramics [18–20]. The latter class of materials is particularly suitable for MOE fabrication, as they can be structured accurately with minimal shrinkage, keeping their transparency at visible and near-infrared (NIR) wavelengths [21–24]. However, most of these materials have a low laser-induced damage threshold (LIDT), as a result of their high organic content [25, 26]. This makes them suitable only for low-power laser applications.

In this paper, we present a novel formulation of organically modified ceramics materials, with improved

LIDT performance, compared to other materials used for MOE fabrication using MPL [25]. The new hybrids are synthesized by reducing their organic content to the minimum amount possible, while still allowing their processing by lithographic techniques, i.e. the removal of the material at the unexposed areas during the structure development step. We validate that they can be structured accurately on flat substrates and on fiber tips by MPL. Moreover, we demonstrate that the formulated resists are suitable for large area ultraviolet light assisted nano-imprint lithography (UV-NIL) processing, allowing for mass-replication and their utilization in optical applications such as diffractive optical elements (DOEs). Finally, we use them to build MOEs such as lenses and axicons on glass substrates and on optical fibers, and we characterize them.

2 Materials and methods

2.1 Material synthesis

Four different photoresists were synthesized based on zirconium-silicon and titanium-silicon inorganic networks. The materials were fabricated from 3-(Trimethoxysilyl) propyl methacrylate (MAPTMS, Sigma-Aldrich), a hybrid monomer bearing photopolymerizable methacrylate moieties and zirconium propoxide, (ZPO, 70% solution in 1-propanol, Sigma-Aldrich) and titanium (IV) isopropoxide (TIPO, 97%, Sigma-Aldrich) were used as an inorganic network former. The molar ratios of MAPTMS to ZPO and TIPO that were studied were 8 : 2 to 7 : 3 for both metal alkoxide precursors. In a typical synthesis, MAPTMS was firstly hydrolyzed by adding HCl, (concentration 0.1 M) at a 1 : 1 molar ratio and the mixture was stirred for 10 min. ZPO or TIPO was then added dropwise in the hydrolyzed MAPTMS monomer, and the mixture was stirred for 30 min. Finally, 2-benzyl-2-(dimethylamino)-4′-morpholinobutyrophenone (Irgacure 369, 97%, Sigma-Aldrich) was used as a photoinitiator (PI) at a 1% wt in respect to the MAPTS monomer. After stirring for 20 more minutes, the materials were filtered using 0.45 μm pores size filters.

Before processing, the samples were dried under vacuum overnight. This resulted in the condensation of the hydroxy-mineral moieties and the formation of the inorganic matrix.

2.2 LIDT characterization

LIDT samples were prepared by spin coating onto fused silica substrates creating a thin film of 1.5 μm and the resultant films were dried in vacuum overnight before photopolymerization using a UV lamp.

The LIDT characterization of the new composites was carried out for two different pulse lengths, namely 10 ns and 300 fs, according to the ISO 21254 standard. The damage threshold was estimated for both the single pulse per site irradiation (1-on-1 test) and a series of pulses with constant energy per site (S-on-1 testing, S = 1000). Depending on dominating failure and pulse duration, single-shot (1-on-1) results might represent either fundamental (intrinsic) material properties [27] or signature of extrinsic (defect driven) damage [28], responsible for initiation laser-induced failure, while multi-shot (S-on-1) testing is used to evaluate fatigue effects attributed to defect generation (bond breaking) [29] and thermal energy accumulation [30]. As in MOE applications, the main damage cause is fatigue, S-on-1 LIDT characterization is used for the benchmarking of different materials and coatings.

The laser characteristics employed in this study are summarized in Table 1.

Fluence was adjusted with a motorized attenuator consisting of a half-wave plate and polarizer.

The online damage detection system was based on optical scattering from the irradiated sample surface. A photodiode sensor was used to track laser-induced surface changes. Damage detecting optical scattering signal was recorded for every pulse.

The off-line inspection of irradiated sites was performed by Nomarski microscopy (BX51, Olympus) after irradiation exposure. Here, the criterion of damage is any visible modifications that can be seen with it. LIDTs have been calculated using a nonlinear fitting procedure based on the maximum-likelihood approach described elsewhere in detail [31]. Estimated error bars correspond to a confidence level of 95%. Distance between neighboring exposition points was fixed to 500 μm to avoid deposition of the damaged (ablated) material on the surrounding surface. The damage threshold of the substrate was always higher than the composites tested and therefore did not influence the results.

2.3 MPL microfabrication

MOEs were fabricated on glass substrates and on the endface of optical fibers.

For the micro-lens fabrication, a home-built experimental setup was employed, where the focused laser beam remained stationary, and the sample moved. The laser source employed was a Femtosecond Fiber Laser (FemtoFiber pro NIR, Toptica Photonics AG) emitting at 780 nm with a pulse duration of 150 fs, average output power 500 mW, and a repetition rate of 80 MHz. A 100× microscope objective lens (Zeiss, Plan Apochromat, N.A. = 1.4) was used to focus the laser beam into the volume of the photosensitive material. Sample movement in the xyz space was achieved using piezoelectric stages (Nanocube, Physik Instrumente). The writing speed was 30 μm/s and the peak intensity at the center of the focal point was approximately 0.5 TW/cm^2. The detailed experimental setup and writing procedure has been described elsewhere [32].

Table 1: Characteristics of the lasers employed in LIDT measurements.

	ns characterization	fs characterization
Central wavelength	1064.0 nm	1030.0 nm
Pulse repetition frequency	100 Hz	200 kHz
Spatial beam profile in the target plane	TEM00	TEM00
Beam diameter in target plane ($1/e^2$)	(230.9 ± 3.7) μm	(74.4 ± 0.4) μm
Pulse duration (FWHM)	(9.6 ± 0.3) ns	300 fs

For the fabrication on the endface of optical fibers, a different set-up was used, employing the same light source, a homemade fiber holder, and a galvanometric scanner. In this case, the structure is printed layer-by-layer, with the focused laser beam moving on the $x-y$ axis, while the sample moves only on the z-axis, to enable the writing of another layer. A 40× microscope objective lens (Zeiss, Plan Apochromat, N.A. = 1.4 Oil DIC) was used to focus the laser beam into the volume of the photosensitive material. Three different designs of axicons were fabricated by using different internal angles, namely 145°, 135°, and 120°. The writing speed was 15 mm/s and the peak intensity at the center of the focal point was approximately 0.67 TW/cm^2. Moreover, the layer thickness (step in z-axis), as well as the hatching (step in xy axes), was set at 100 nm. The results are presented in Figure 4. The fiber holder and the 3D writing procedure have been described elsewhere [9].

After the completion of the component building process, the samples were developed for 30 min in 4-methyl-2-pentanone and were further rinsed with 2-propanol.

2.4 UV-NIL patterning

UV-NIL patterning was carried out by Nanotypos (Thessaloniki, Greece) [33]. A silicon master mold comprising various two-dimensional diffractive grating structures and DOEs was fabricated by electron-beam lithography and reactive ion etching processes. To promote separation during the UV-NIL step, the Si master molds were treated with a low surface energy antisticking agent (Optool DSX, Daikin chemical) based on fluorosilanes. This layer has a thickness of about 3 nm and results in a surface free energy of 11 ± 0.5 mN/m, which prevents any adhesion effect, which could contaminate the replicated step. During our experimental work, our working mold was a soft PDMS mold which was a negative replicate from the Si master mold. PDMS was realized by mixing the curing and base material in a 1 : 10 ratio, respectively.

The hybrid photoresist layer was spin coated on a glass substrate while the assembly (PDMS mold and substrate/resist) was bought into physical contact (holding pressure 1 bar) inside the chamber of a commercial nanoimprint lithography tool (CNI tool from NILTechnology Aps. Denmark) at a temperature of 70 °C for 120 min. Following the prebaking process, a UV light irradiation exposure was carried out for 12 min followed by a post exposure bake at 70 °C for 180 min. The topographical characterization of the imprinted patterns was observed by scanning electron microscopy (SEM) in the top and tilted view (Figure 3).

2.5 Spectral characterization

The absorbance spectra of thin films of all four synthesized materials were recorded in the 300–1300 nm spectral range using a PerkinElmer UV–vis spectrometer.

3 Results and discussion

3.1 Absorption spectra

The UV–vis spectra of the ZPO and TIPO material thin films after photopolymerization are shown in Figure 1. All synthesized composites exhibit zero absorbance above 500 nm and thus are fully transparent in the NIR and visible part of the spectrum, making them suitable for transmissive MOE applications using such wavelengths. In all cases, the materials start to absorb below 500 nm with identical absorption curves regardless of their composition. This is attributed to the PI Irgacure 369 that they contain which has a typical absorbance between 250 and 430 nm.
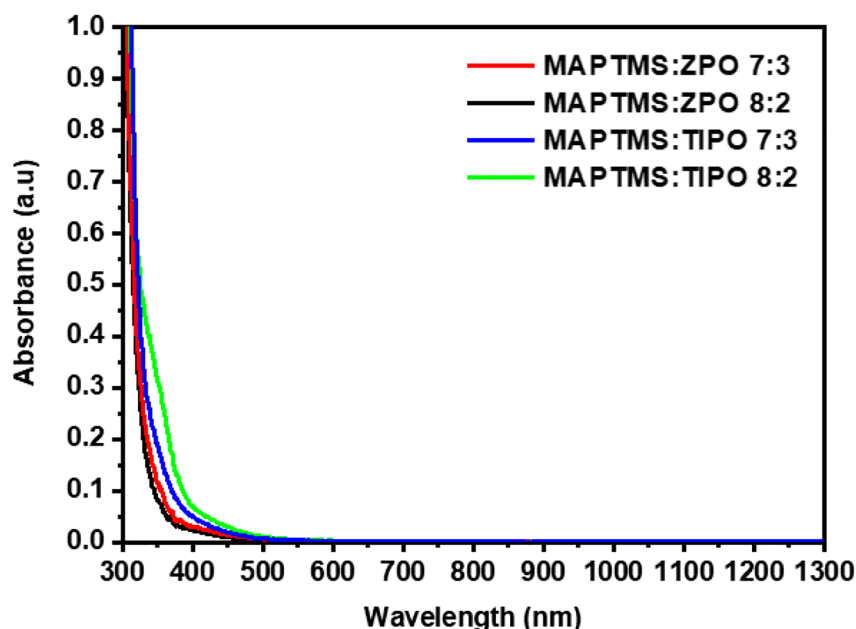
Figure 1: Absorption spectra of the ZPO and TIPO hybrid photoresists. The red and black line corresponds to the MAPTMS : ZPO 7 : 3 and 8 : 2 molar ratio material, respectively, while the blue and green line corresponds to the MAPTMS : TIPO 7 : 3 and 8 : 2 molar ratio, respectively.

3.2 LIDT measurements

As discussed earlier, LIDT characterization was done by using both ns and fs pulse durations, using 1 and 1000 pulses.

The results of the ns investigation are shown in Table 2. In the same table, the LIDT characterization of ORMOCOMP™ and SU-8 is presented [25], for comparison reasons. Both these materials are widely used in MPL and NIL [34, 35].

As it can be seen, all the new composites have a considerably higher damaged threshold than the reference materials, especially in the S-on-1 test, which is the one that defines the suitability of the material for optical applications. The material exhibiting the highest LIDT is the one containing MAPTMS : ZPO 8 : 2, whose damage threshold is 1.36 times and 9.35 times higher than ORMOCOMP™, for the 1-on-1 and S-on-1 test, respectively. This is not surprising, as ZrO_2 is the material of choice for high-power optical components, and the MAPTMS : ZPO composites are likely to contain ZrO_2 nanoparticles. This is confirmed by the residual fluorescence in MAPTMS : ZPO composites [36].

The results of the fs investigation are shown in Table 3. Here, the zirconium composites again have higher LIDT than the others. The MAPTMS : ZPO 7 : 3 composite has slightly higher LIDT than the MAPTMS : ZPO 8 : 2, exhibiting a damage threshold is 1.2 times and 2.05 times higher than ORMOCOMP™, for the 1-on-1 and S-on-1 test, respectively.

When directly comparing LIDTs of the investigated samples, titania-based composites did not perform as well as the zirconia compounds. As it is shown in Figure 1 titania-based coatings also exhibit a lower bandgap. Lower bandgap can be directly related to laser damage resistance, as multiphoton processes are typically involved [37]. Also, as it can be seen, the lack of organic compounds seems to affect fatigue properties and long-term damage performance. Accordingly, oxide-only materials are preferred for free-form micro-optics for high-power laser applications, however, they cannot be processed by MPL and UV-NIL

Table 2: ns LIDT characterization.

Material	Damage Threshold (J/cm²) (1-on-1)	Damage threshold (J/cm²) (1000-on-1)
MAPTMS : ZPO 7 : 3	26.9 (+2.66, −4.42)	2.75 (+0.28, −0.52)
MAPTMS : ZPO 8 : 2	33.48 (+2.51, −4.04)	12.63 (+1.07,−1.80)
MAPTMS : TIPO 7 : 3	23.97 (+2.14, −3.42)	2.75 (+0.28, −0.52)
MAPTMS : TIPO 8 : 2	28.36 (+2.14, −3.43)	1.93 (+0.15, −0.23)
ORMOCOMP™ [25]	24.60 ± 2.73	1.35 ± 1.05
SU-8 2015 [25]	19.77 ± 2.29	0.49 ± 0.09

Table 3: fs LIDT characterization.

Material	Damage threshold (J/cm²) (1-on-1)	Damage threshold (J/cm²) (1000-on-1)
MAPTMS : ZPO 7 : 3	2.011 ± 0.088	0.678 ± 0.025
MAPTMS : ZPO 8 : 2	1.870 ± 0.084	0.552 ± 0.032
MAPTMS : TIPO 7 : 3	1.652 ± 0.071	0.573 ± 0.024
MAPTMS : TIPO 8 : 2	1.124 ± 0.055	0.244 ± 0.013
ORMOCOMP™ [25]	1.67 ± 0.65	0.33 ± 0.13
SU-8 2015 [25]	1.48 ± 0.41	0.17 ± 0.05

[38, 39]. For femtosecond pulse durations, both 1-on-1 and 1000-on-1 LIDT, there was limited smooth damage morphology indicating deterministic damage governed by electronic absorption processes and color center formation within the entire matrix of coating material. In the case of nanosecond pulses, damages were rather catastrophic, originated from localized absorption centers (sporadic defects) embedded either within coating or substrate thus indicating some inhomogeneity. Such defects could be attributed to self-forming clusters of unoxidized absorbing material or polishing defects embedded within substrates. For nanosecond irradiation, some of the zirconia-compound-based sample sites withstand 1000 pulses and survived at fluence >60 J/cm² thus also showing the potential of these materials for further improvement (removal of defects). That is not trivial and could be achieved by further purification of the photoresist composite materials (all were used as purchased), and by performing the preparation and processing of the materials in a clean-room environment.

3.3 UV-NIL patterning

Figure 2 shows photographs of some of the gratings fabricated by UV-NIL, using some of the photoresists developed. It is clear that the new composites can be processed over large areas without breaking or cracking. Figures 3 and 4 show SEM images of some of the relief surface structures and a DOE, respectively, made using the MAPTMS : ZPO 8 : 2 composite. The composite can be UV-NIL printed with accuracy, making it a material suitable for the mass fabrication of MOEs for high-power laser applications.

3.4 3D MPL microfabrication

To investigate the performance of the composites in 3D multi-photon lithography, micro-optical structures were fabricated, using the composite MAPTMS : ZPO 8 : 2, which
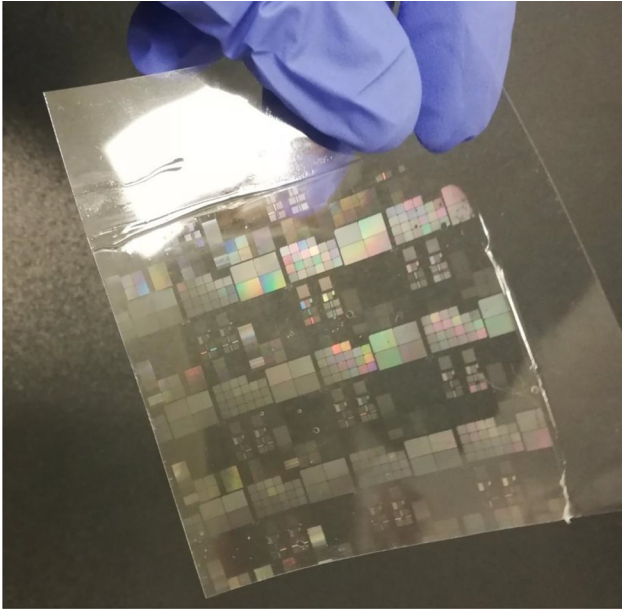
Figure 2: Patterned areas using the new hybrid photoresist MAPTMS : ZPO 8 : 2 made by NIL.

showed the most promising LIDT performance. Plano-convex microlenses were fabricated on flat surfaces and micro-axicons were fabricated on flat surfaces as well as on optical fibers.

Plano-convex microlenses were fabricated with a radius of curvature of 100 μm and a diameter size of 90 μm. Figure 5 depicts images of the fabricated lenses. Figure 5a shows an SEM image of the lens in the top view, while Figure 5b shows the same lens at the tilted view. Figure 5c shows an optical microscope image (taken with Dino-Lite digital microscope [AM7915MZT, AnMo Electronics Corporation, Taiwan]) of the same lens in transmission mode, while in Figure 5d the focusing of the transmitted light from the microlens can be seen by changing the focal point to a plane above the lens. The focused beam spot size was measured using DinoCapture 2.0 software and was found to be 15 μm. The focal length was calculated to be approximately 200 μm, using the formula $f = \frac{rc}{n-1}$ [40], where rc is the radius of curvature and n is the refractive index of the material, in our case $n \sim 1.52$.
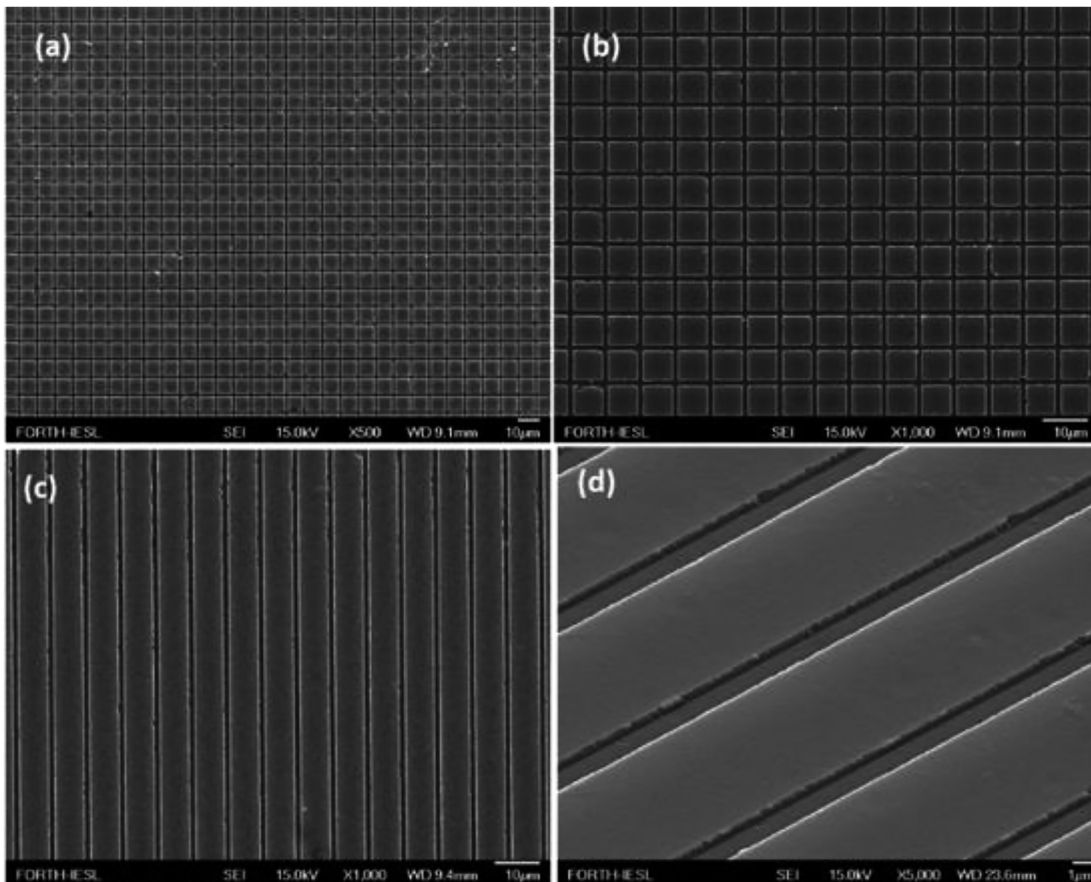

Figure 3: Representative SEM images from the hybrid photoresist consisting of MAPTMS : ZPO 8 : 2 molar ratio (a and b) images of a patterned area consisting of squares (c and d) a patterned area consisting of lines.
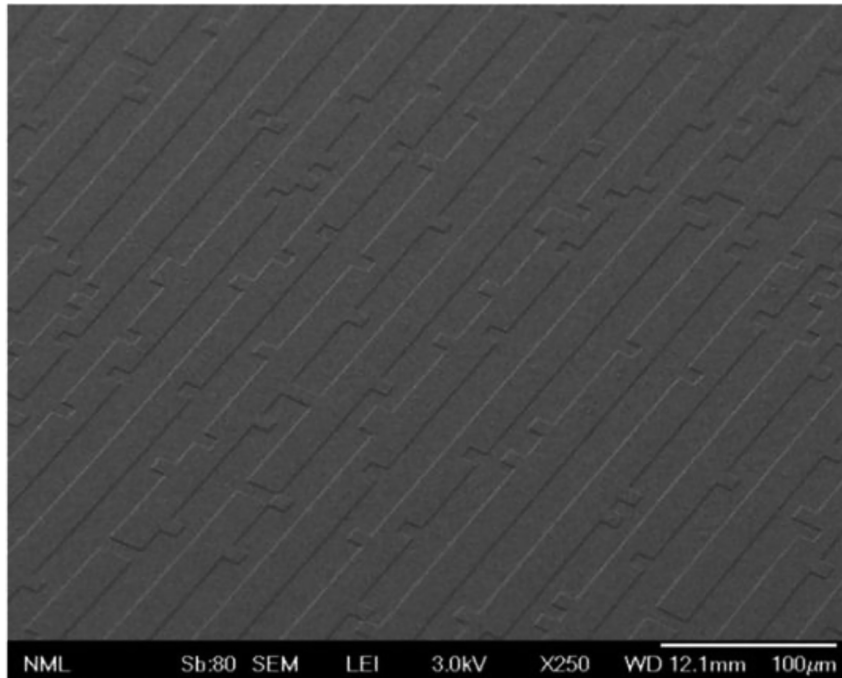
Figure 4: A DOE made by UV-NIL lithography of the MAPTMS : ZPO 8 : 2 composite.
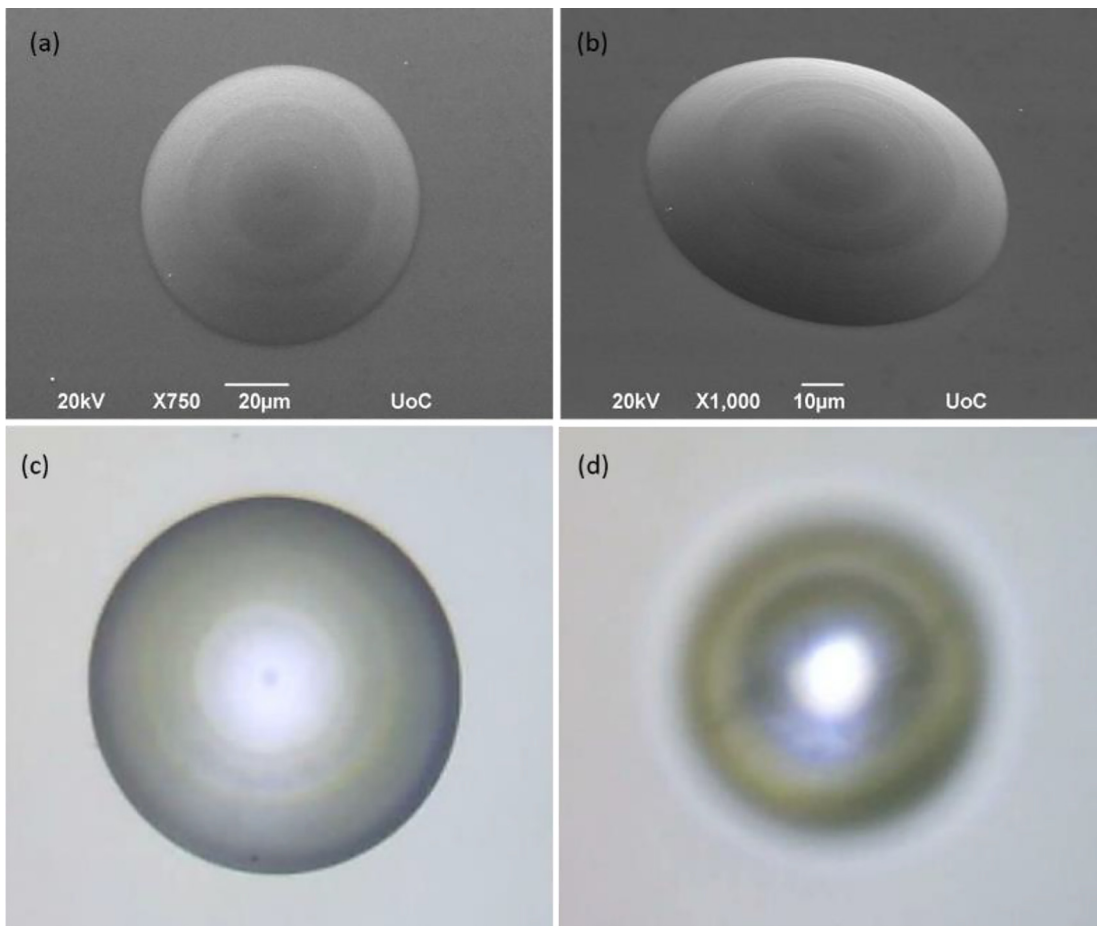
Figure 5: (a) SEM image of a printed microlens using the MPL technique (b) tilted view of the microlens (c) optical microscope image of the same lens (d) optical microscope image of the microlens focusing on a plane above the lens, where the focusing of the transmitted light can be observed.
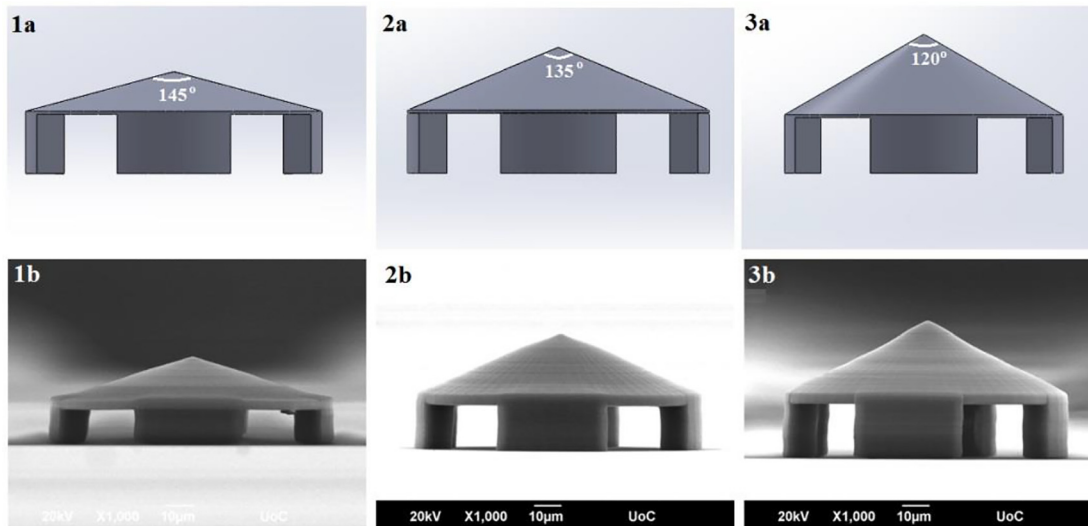
Figure 6: (1a), (2a), and (3a) present the CAD images of 100 μm-diameter axicons with inset angles of 145°, 135°, and 120°, respectively. Scanning electron microscopy (SEM) images of fabricated axicons are presented in (1b), (2b), and (3b).
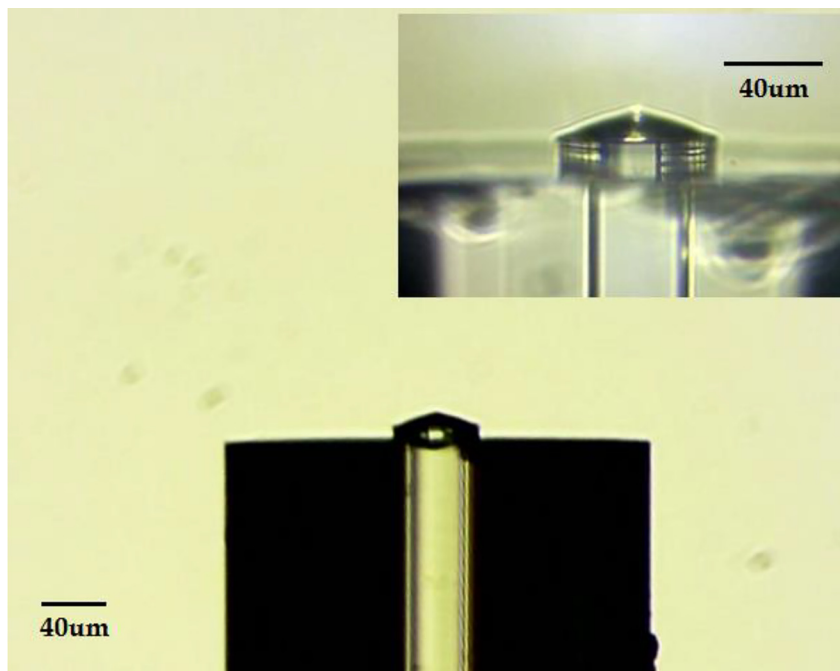

Figure 7: Digital microscope images at 220× magnification of the fabricated axicons on the endface of the optical fiber.

As it is clear the new composites can be structured accurately using 3D MPL and are being candidates for the fabrication of MOEs with even more complicated designs.

Figure 6 shows the computer-aided designs (CAD) and respective SEM images of a series of axicons with different internal angles made using the MAPTMS : ZPO 8 : 2 composite, on a glass substrate. Axicons with the same internal angles were subsequently fabricated on the endface of a multimode optical fiber. The purpose of the support

structures was to allow the Gaussian beam to expand before entering the axicon.

All the MOEs fabricated on flat glass surfaces show integrity and stability. Figure 7 shows a digital microscope image of axicons fabricates on the tip of an optical fiber. Characterization of the axicon was performed to prove its ability to produce non-diffracting beams. Initially, a He–Ne laser (632 nm) was coupled to the fiber using a focusing lens (40× aspheric lens with A coating). The occurrence of non-diffracted beam is monitored using a magnifying lens
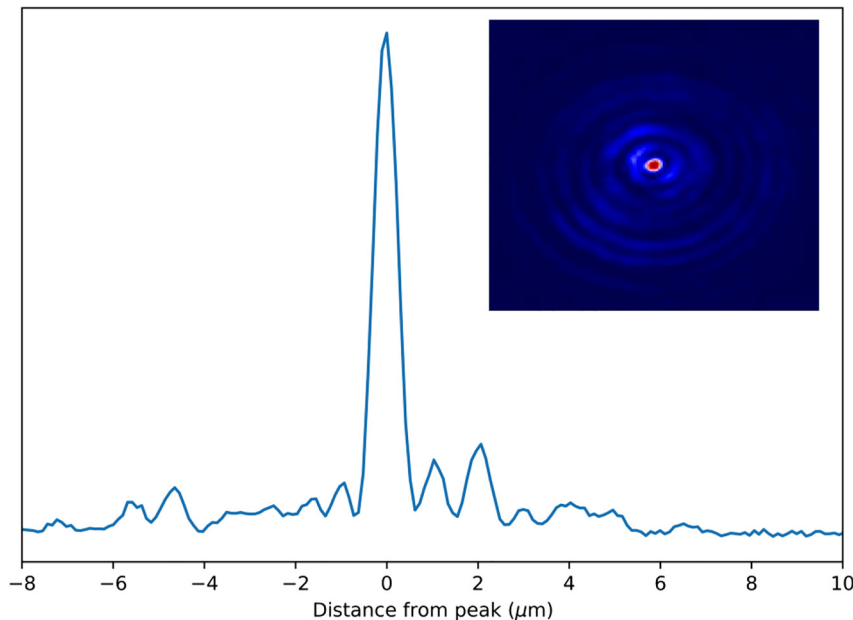
Figure 8: Radial intensity profile corresponding to the transverse profile of the generated nondiffracting beam (inset).

(60× aspheric lens, A-coated) and a visible-infrared camera (WinCamD, pixel dimensions 9.3×9.3 μm^2). The magnifying lens and the camera are mounted on a linear translation stage (Thorlabs). The distance between the magnifying lens and the camera is kept fixed giving a magnification factor of 90. Figure 8 shows the radial intensity distribution and the corresponding transverse profile (inset) of the generated nondiffracting (Bessel) beam from the above explained setup. The transverse profile depicts a zero-order Bessel function pattern and the corresponding radial intensity profile mimics, to a large degree, the expected pattern from such a transverse profile.

4 Conclusions

To sum up, a series of photosensitive, transparent zirconium and titanium silicates with minimal organic content were synthesized and investigated for their LIDT and their suitability for processing using NIL and MPL. All materials exhibited high LIDT, with the zirconia silicates exhibiting higher LIDT values. The materials showed good processability using MPL and NIL, and over large areas, with no signs of cracking or breaking. The ability of the newly synthesized hybrids to be processed accurately with MPL and NIL could give rise to the mass production of MOEs and DOEs with elevated complexity, whose fabrication is limited up to now with the existing techniques. Microlenses and micro-axicons were fabricated successfully using these materials via MPL. Axicons on fiber endfaces

were made and characterized in their ability to produce nondiffracting beams. Our results show that these materials as candidates for the fabrication of MOEs for high-power laser applications.

References

[1] R. S. Muller and K. Y. Lau, "Surface-micromachined microoptical elements and systems," *Proc. IEEE*, vol. 86, no. 8, pp. 1705–1720, 1998.
[2] T. Gissibl, S. Thiele, A. Herkommer, and H. Giessen, "Two-photon direct laser writing of ultracompact multi-lens objectives," *Nat. Photonics*, vol. 10, no. 8, pp. 554–560, 2016.
[3] P. I. Dietrich, M. Blaicher, I. Reuter, et al., "In situ 3D nanoprinting of free-form coupling elements for hybrid photonic integration," *Nat. Photonics*, vol. 12, no. 4, pp. 241–247, 2018.

[4] M.-S. Kim, T. Scharf, S. Mühlig, C. Rockstuhl, and H. P. Herzig, "Engineering photonic nanojets," *Opt Express*, vol. 19, no. 11, pp. 10206–10220, 2011.

[5] W. Hadibrata, H. Wei, S. Krishnaswamy, and K. Aydin, "Inverse design and 3D printing of a metalens on an optical fiber tip for direct laser lithography," *Nano Lett.*, vol. 21, no. 6, pp. 2422–2428, 2021.

[6] M. Plidschun, H. Ren, Jisoo Kim, R. Förster, S. A. Maier, and M. A. Schmidt, "Ultrahigh numerical aperture meta-fibre for flexible optical trapping," *Light Sci. Appl.*, vol. 10, no. 1, p. 57, 2021.

[7] S. Varapnickas, S. C. Thodika, F. Moroté, S. Juodkazis, M. Malinauskas, and E. Brasselet, "Birefringent optical retarders from laser 3D-printed dielectric metasurfaces," *Appl. Phys. Lett.*, vol. 118, no. 15, p. 5, 2021.

[8] G. S. Sokolovskii, V. Melissinaki, K. A. Fedorova, et al., "3D laser nano-printing on fibre paves the way for super-focusing of multimode laser radiation," *Sci. Rep.*, vol. 8, p. 14618, 2018.

[9] V. Melissinaki, M. Farsari, and S. Pissadakis, "A fiber-endface, fabry-perot vapor microsensor fabricated by multiphoton polymerization," *IEEE J. Sel. Top. Quant. Electron.*, vol. 21, no. 4, 2015, Art no. 5600110.

[10] J. Bürger, J. Kim, B. Jang, J. Gargiulo, M. A. Schmidt, and S. A. Maier, "Ultrahigh-aspect-ratio light cages: fabrication limits and tolerances of free-standing 3D nanoprinted waveguides," *Opt. Mater. Express*, vol. 11, no. 4, pp. 1046–1057, 2021.

[11] V. Melissinaki, O. Tsilipakos, M. Kafesaki, M. Farsari, and S. Pissadakis, "Micro-ring resonator devices prototyped on optical fiber tapers by multi-photon lithography," *IEEE J. Sel. Top. Quant. Electron.*, vol. 27, no. 6, pp. 1–7, 2021.

[12] J. Moughames, X. Porte, M. Thiel, et al., "Three-dimensional waveguide interconnects for scalable integration of photonic neural networks," *Optica*, vol. 7, no. 6, pp. 640–646, 2020.

[13] A. Bertoncini and C. Liberale, "3D printed waveguides based on photonic crystal fiber designs for complex fiber-end photonic devices," *Optica*, vol. 7, no. 11, pp. 1487–1494, 2020.

[14] P. I. Dietrich, R. J. Harris, M. Blaicher, et al., "Printed freeform lens arrays on multi-core fibers for highly efficient coupling in astrophotonic systems," *Opt Express*, vol. 25, no. 15, pp. 18288–18295, 2017.

[15] V. Melissinaki, O. Tsilipakos, M. Kafesaki, M. Farsari, and S. Pissadakis, "Micro-ring resonator devices prototyped on optical fiber tapers by multi-photon lithography," *IEEE J. Sel. Top. Quant. Electron.*, vol. 27, no. 6, 2021. https://doi.org/10.1109/jstqe.2021.3062716.

[16] E. Skliutas, M. Lebedevaite, E. Kabouraki, et al., "Polymerization mechanisms initiated by spatio-temporally confined light," *Nanophotonics*, vol. 10, pp. 1211–1242, 2021.

[17] M. Malinauskas, A. Žukauskas, S. Hasegawa, et al., "Ultrafast laser processing of materials: from science to industry," *Light Sci. Appl.*, vol. 5, p. 14, 2016.

[18] A. Koroleva, A. Deiwick, A. El-Tamer, et al., "In vitro development of human iPSC-derived functional neuronal networks on laser-fabricated 3D scaffolds," *ACS Appl. Mater. Interfaces*, vol. 13, no. 7, pp. 7839–7853, 2021.

[19] L. Tytgat, A. Dobos, M. Markovic, et al., "High-resolution 3D bioprinting of photo-cross-linkable recombinant collagen to serve tissue engineering applications," *Biomacromolecules*, vol. 21, no. 10, pp. 3997–4007, 2020.

[20] G. Weisgrab, O. Guillaume, Z. Guo, et al., "3D Printing of large-scale and highly porous biodegradable tissue engineering scaffolds from poly(trimethylene-carbonate) using two-photon-polymerization," *Biofabrication*, vol. 12, no. 4, 2020. https://doi.org/10.1088/1758-5090/abb539.

[21] M. Farsari, M. Vamvakaki, and B. N. Chichkov, "Multiphoton polymerization of hybrid materials," *J. Opt.*, vol. 12, no. 12, 2010, Art no. 124001.

[22] F. Burmeister, S. Steenhusen, R. Houbertz, U. D. Zeitner, S. Nolte, and A. Tünnermann, "Materials and technologies for fabrication of three-dimensional microstructures with sub-100 nm feature sizes by two-photon polymerization," *J. Laser Appl.*, vol. 24, no. 4, 2012, Art no. 042014.

[23] S. Steenhusen, F. Burmeister, M. Groß, G. Domann, R. Houbertz, and S. Nolte, "Heterogeneous microoptical structures with sub-micrometer precision," *Thin Solid Films*, vol. 668, pp. 74–80, 2018.

[24] T. Stichel, B. Hecht, S. Steenhusen, R. Houbertz, and G. Sextl, "Two-photon polymerization setup enables experimental mapping and correction of spherical aberrations for improved macroscopic structure fabrication," *Opt Lett.*, vol. 41, no. 18, pp. 4269–4272, 2016.

[25] A. Žukauskas, G. Batavičiūtė, M. Ščiuka, T. Jukna, A. Melninkaitis, and M. Malinauskas, "Characterization of photopolymers used in laser 3D micro/nanolithography by means of laser-induced damage threshold (LIDT)," *Opt. Mater. Express*, vol. 4, no. 8, pp. 1601–1616, 2014.

[26] A. Butkutė, L. Čkanavičius, G. Rimšelis, et al., "Optical damage thresholds of microstructures made by laser three-dimensional nanolithography," *Opt Lett.*, vol. 45, no. 1, pp. 13–16, 2020.

[27] M. Mero, J. Liu, W. Rudolph, D. Ristau, and K. Starke, "Scaling laws of femtosecond laser pulse induced breakdown in oxide films," *Phys. Rev. B*, vol. 71, no. 11, p. 115109, 2005.

[28] M. Sozet, J. Néauport, E. Lavastre, N. Roquin, L. Gallais, and L. Lamaignère, "Laser damage density measurement of optical components in the sub-picosecond regime," *Opt Lett.*, vol. 40, no. 9, pp. 2091–2094, 2015.

[29] A. E. Chmel, "Fatigue laser-induced damage in transparent materials," *Mater. Sci. Eng, B*, vol. 49, no. 3, pp. 175–190, 1997.

[30] X. Jia and X. Zhao, "Thermal accumulation at kilohertz repetition rates inside fused silica under ultrafast laser irradiation," *Opt Lett.*, vol. 45, no. 13, pp. 3390–3393, 2020.

[31] G. Batavičiūtė, P. Grigas, L. Smalakys, and A. Melninkaitis, "Revision of laser-induced damage threshold evaluation from damage probability data," *Rev. Sci. Instrum.*, vol. 84, no. 4, 2013, Art no. 045108.

[32] A. N. Giakoumaki, G. Kenanakis, A. Klini, et al., "3D micro-structured arrays of ZnO nanorods," *Sci. Rep.*, vol. 7, p. 2100, 2017.

[33] www.nanotypos.com.

[34] R. Houbertz, L. Fröhlich, M. Popall, et al., "Inorganic-organic hybrid polymers for information technology: from planar technology to 3D nanostructures," *Adv. Eng. Mater.*, vol. 5, no. 8, pp. 551–555, 2003.

[35] Z. M. Tong, F. Niu, Z. Jian, et al., "Micro-refractive optical elements fabricated by multi-exposure lithography for laser speckle reduction," *Opt Express*, vol. 28, no. 23, pp. 34597–34605, 2020.

[36] G. Flamourakis, A. Kordas, G. D. Barmparis, A. Ranella, and M. Farsari, "Low-autofluorescence, transparent composite for multiphoton 3D printing," *Opt. Mater. Express*, vol. 11, no. 3, pp. 801–813, 2021.

[37] B. Mangote, L. Gallais, M. Commandré, et al., "Femtosecond laser damage resistance of oxide and mixture oxide optical coatings," *Opt Lett.*, vol. 37, no. 9, pp. 1478–1480, 2012.

[38] A. Vyatskikh, R. C. Ng, B. Edwards, R. M. Briggs, and J. R. Greer, "Additive manufacturing of high-refractive-index, nanoarchitected titanium dioxide for 3D dielectric photonic crystals," *Nano Lett.*, vol. 20, no. 5, pp. 3513–3520, 2020.

[39] D. Gailevicius, V. Padolskytė, L. Mikoliūnaitė, S. Šakirzanovas, S. Juodkazis, and M. Malinauskas, "Additive-manufacturing of 3D glass-ceramics down to nanoscale resolution," *Nanoscale Horiz.*, vol. 4, no. 3, pp. 647–651, 2019.

[40] H.-T. Hsieh, V. Lin, J.-L. Hsieh, and G.-D. John Su, "Design and fabrication of long focal length microlens arrays," *Opt Commun.*, vol. 284, no. 21, pp. 5225–5230, 2011.